

## Article

# The Effects of Charged Amino Acid Side-Chain Length on Diagonal Cross-Strand Interactions between Carboxylate- and Ammonium-Containing Residues in a $\beta$ -Hairpin

Jing-Yuan Chang <sup>1</sup>, Yen-Jin Pan <sup>1</sup>, Pei-Yu Huang <sup>1</sup>, Yi-Ting Sun <sup>1</sup>, Chen-Hsu Yu <sup>1</sup>, Zhi-Jun Ning <sup>1</sup>, Shou-Ling Huang <sup>2</sup>, Shing-Jong Huang <sup>2</sup> and Richard P. Cheng <sup>1,\*</sup> 

<sup>1</sup> Department of Chemistry, National Taiwan University, Taipei 10617, Taiwan; r08223149@ntu.edu.tw (J.-Y.C.); r03223211@ntu.edu.tw (Y.-J.P.); r03223210@ntu.edu.tw (P.-Y.H.); b99203034@ntu.edu.tw (Y.-T.S.); r05223205@ntu.edu.tw (C.-H.Y.); r09223205@ntu.edu.tw (Z.-J.N.)

<sup>2</sup> Instrumentation Center, National Taiwan University, Taipei 10617, Taiwan; shouling@ntu.edu.tw (S.-L.H.); shingjonghuang@ntu.edu.tw (S.-J.H.)

\* Correspondence: rpcheng@ntu.edu.tw

**Abstract:** The  $\beta$ -sheet is one of the common protein secondary structures, and the aberrant aggregation of  $\beta$ -sheets is implicated in various neurodegenerative diseases. Cross-strand interactions are an important determinant of  $\beta$ -sheet stability. Accordingly, both diagonal and lateral cross-strand interactions have been studied. Surprisingly, diagonal cross-strand ion-pairing interactions have yet to be investigated. Herein, we present a systematic study on the effects of charged amino acid side-chain length on a diagonal ion-pairing interaction between carboxylate- and ammonium-containing residues in a  $\beta$ -hairpin. To this end, 2D-NMR was used to investigate the conformation of the peptides. The fraction folded population and the folding free energy were derived from the chemical shift data. The fraction folded population for these peptides with potential diagonal ion pairs was mostly lower compared to the corresponding peptide with a potential lateral ion pair. The diagonal ion-pairing interaction energy was derived using double mutant cycle analysis. The Asp2-Dab9 (Asp: one methylene; Dab: two methylenes) interaction was the most stabilizing ( $-0.79 \pm 0.14$  kcal/mol), most likely representing an optimal balance between the entropic penalty to enable the ion-pairing interaction and the number of side-chain conformations that can accommodate the interaction. These results should be useful for designing  $\beta$ -sheet containing molecular entities for various applications.

**Keywords:** peptide;  $\beta$ -hairpin; diagonal interaction; ion-pairing interaction; charged amino acid; side-chain length



**Citation:** Chang, J.-Y.; Pan, Y.-J.; Huang, P.-Y.; Sun, Y.-T.; Yu, C.-H.; Ning, Z.-J.; Huang, S.-L.; Huang, S.-J.; Cheng, R.P. The Effects of Charged Amino Acid Side-Chain Length on Diagonal Cross-Strand Interactions between Carboxylate- and Ammonium-Containing Residues in a  $\beta$ -Hairpin. *Molecules* **2022**, *27*, 4172. <https://doi.org/10.3390/molecules27134172>

Academic Editor: Marilisa Leone

Received: 28 January 2022

Accepted: 23 March 2022

Published: 29 June 2022

**Publisher's Note:** MDPI stays neutral with regard to jurisdictional claims in published maps and institutional affiliations.



**Copyright:** © 2022 by the authors. Licensee MDPI, Basel, Switzerland. This article is an open access article distributed under the terms and conditions of the Creative Commons Attribution (CC BY) license (<https://creativecommons.org/licenses/by/4.0/>).

## 1. Introduction

The  $\beta$ -sheet is one of the common protein secondary structures, with 23% of the protein residues adopting a  $\beta$ -sheet conformation [1–3]. Aberrant aggregation of  $\beta$ -sheets form amyloid fibrils involved in a number of neurodegenerative diseases including Alzheimer's disease [4,5], Huntington's disease [6,7], and Parkinson's disease [8]. As such, studies on  $\beta$ -sheet stability and formation may provide insight into the emergence and treatment of these neurodegenerative diseases.

$\beta$ -Sheet stability is determined by both the thermodynamic sheet propensity of the constituting residues [9,10] and cross-strand interactions [11–13]. A survey focusing on antiparallel  $\beta$ -sheets highlighted the importance of lateral cross-strand interactions between oppositely charged residues [11]. Accordingly, lateral cross-strand interactions have been studied in various sheet-containing host systems, including the protein G B1 domain [14,15], a zinc finger domain [16], and  $\beta$ -hairpins [17–27]. In the protein G B1 domain system, both lateral Glu-Lys and the Glu-Arg interactions provided approximately 1.0 kcal/mol stabilization based on thermal denaturation experiments [14]. In the zinc-finger system,

the lateral cross-strand interaction between negatively charged residues (Asp and Glu) and positively charged residues (Arg and Lys) were 0.02–0.48 kcal/mol based on competitive metal ion binding studies [16]. In  $\beta$ -hairpins, lateral cross-strand Glu–Lys ion-pairing interactions provided 0.1–0.3 kcal/mol stabilization based on NMR studies [20,22,23]. Furthermore, various types of lateral cross-strand interactions have been investigated in  $\beta$ -hairpins, including hydrophobics [17,24], electrostatics [17,20,22,25–27], and aromatic  $\pi$ – $\pi$  interactions [21,22]. Nonetheless, statistical studies showed that diagonal cross-strand interactions are much more significant, compared to lateral cross-strand interactions across antiparallel  $\beta$ -strands [12].

Diagonal cross-strand interactions are enabled by the inherent right-handed twist of  $\beta$ -sheet structures [19,27,28]. Accordingly, a number of diagonal cross-strand interactions have been investigated in  $\beta$ -hairpins, including hydrophobics [24], cation– $\pi$  [29–32], carbohydrate– $\pi$  [33,34], and amide– $\pi$  interactions [35]. These diagonal cross-strand interactions stabilized the  $\beta$ -hairpin structure by 0.1–1.0 kcal/mol [24,29–35]. Surprisingly, the diagonal cross-strand interactions between oppositely charged residues (i.e., ion-pairing interactions) have yet to be investigated. Herein, we present a systematic study on the effects of charged amino acid side-chain length on diagonal cross-strand interactions between carboxylate- and ammonium-containing residues in a  $\beta$ -hairpin.

## 2. Results

### 2.1. Peptide Design and Synthesis

The experimental HPDZbbXaa peptides were designed based on Gellman's YKL peptide [19] and the HPTZbbXaa hairpin peptides described in our previous studies (Figure 1) [3,25,26]. A diagonal cross-strand cation– $\pi$  interaction was observed in the parent YKL  $\beta$ -hairpin peptide [19]. Furthermore, diagonal cross-strand NOEs were observed between positions 2 and 9 in the HPTZbbXaa peptides [3,25–27]. Therefore, the Tyr2 (in peptide YKL) was replaced with negatively charged carboxylate-containing residues to interact with the positively charged ammonium-containing residues at position 9. The Glu4 (in peptide YKL) was replaced with Thr to maintain the  $\beta$ -structure based on the high thermodynamic sheet propensity of Thr [9,10] and to remove the potential lateral ion-pairing interaction with position 9. An acetyl group and a carboxamide group were incorporated at the N- and C-termini, respectively, to minimize unexpected interactions involving the charged termini [17]. To investigate the effects of charged amino acid side-chain length on diagonal cross-strand ion-pairing interactions, the negatively charged carboxylate-containing residues (Zbb = Asp, Glu, Aad) and positively charged ammonium-containing residues (Xaa = Dap, Dab, Orn, Lys) were incorporated at positions 2 and 9, respectively, to give the experimental HPDZbbXaa peptides (Figure 1). The experimental peptides were named HPDZbbXaa, representing a hairpin peptide to study the diagonal interactions, followed by the negatively charged Zbb residue at position 2 and the positively charged Xaa residue at position 9.

The fully folded reference peptides HPDFZbbXaa and the fully unfolded reference peptides HPDUZbbXaa were required to determine the fraction folded population of the experimental HPDZbbXaa peptides (Figure 1b) [3,19,25–27,36–38]. The fully folded reference HPDFZbbXaa peptides were designed by introducing cysteines at both the N- and C-termini of experimental HPDZbbXaa peptides to form intramolecular disulfide bonds [3,19,25–27,36–38]. The fully unfolded reference HPDUZbbXaa peptides were designed by replacing DPro with LPro at position 6 of the experimental HPDZbbXaa peptides, to disrupt the  $\beta$ -hairpin conformation [3,19,25–27,36–38].

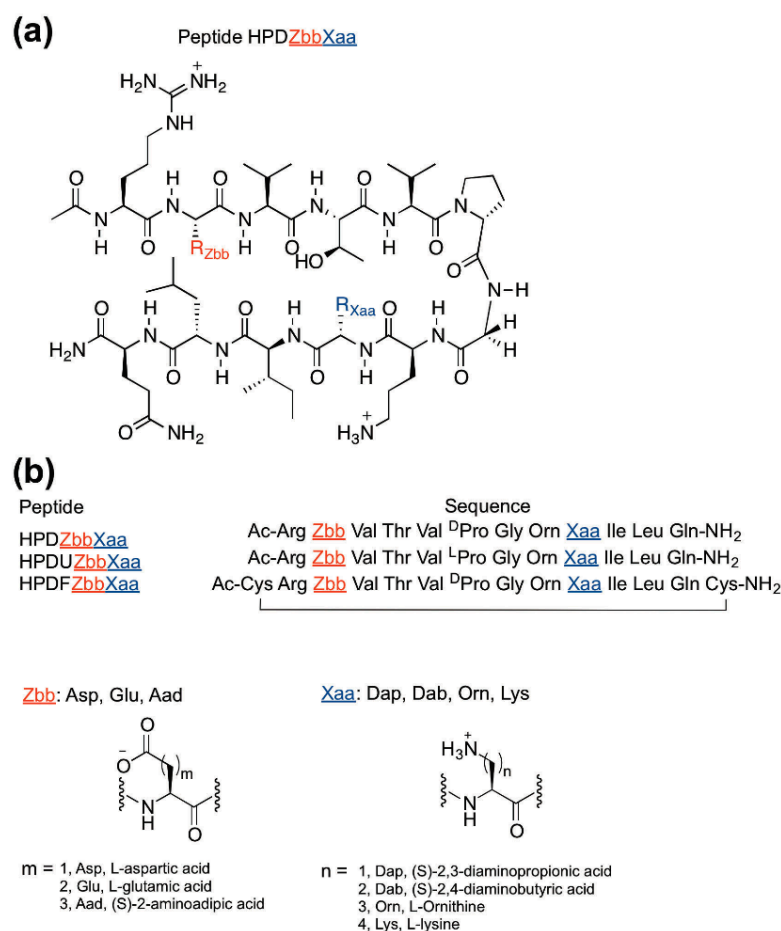


**Figure 1.** Design of peptides to study the effects of charged amino acid side-chain length on diagonal cross-strand ion-pairing interactions: (a) the chemical structure of the experimental HPDZbbXaa peptides; (b) the sequences of the experimental HPDZbbXaa peptides, the fully unfolded reference HPDUZbbXaa peptides, and the fully folded reference HPDFZbbXaa peptides.

The peptides were synthesized by solid-phase peptide synthesis using Fmoc-based chemistry [39,40]. The intramolecular disulfide bond in the fully folded reference HPDFZbbXaa peptides was formed via charcoal-mediated air oxidation [41]. All peptides were purified by reverse-phase high-performance liquid chromatography (RP-HPLC) to higher than 95% purity (except for HPDAspDap, HPDAspDab, HPDGluDap, HPDGluDab, and HPDAadDab, which were purified to higher than 90% purity), and confirmed by matrix-assisted laser desorption ionization time-of-flight (MALDI-TOF) mass spectrometry.

## 2.2. Peptide Structure Characterization by NMR Spectroscopy

The peptides were analyzed by two-dimensional NMR spectroscopy including total correlation spectroscopy (TOCSY), double-quantum filtered-correlated spectroscopy (DQF-COSY), and rotating-frame nuclear Overhauser spectroscopy (ROESY) at 298 K. Sequence-specific assignments of the chemical shifts were performed based on the TOCSY and ROESY spectra (Tables S1–S36) [42]. The number of major spin systems was consistent with the number of residues in each peptide. Weak cross-peaks corresponding to minor conformations were observed in the TOCSY spectra for many of the HPDZbbXaa and HPDUZbbXaa peptides. Since the NMR spectra (chemical shift and peak width) of analogous hairpin peptides did not change with concentration (20  $\mu$ M to 10 mM) [3,19,43,44], the peptides in this study (0.9–10.1 mM) should not aggregate in solution. Accordingly, the experimental data should reflect the intramolecular interactions with minimal interference from intermolecular interactions.

The chemical shift dispersion of the peptides was evaluated using the chemical shift ranges of the HN and H $\alpha$  protons, and the standard deviations of the average chemical shifts of the HN and H $\alpha$  protons (Table 1). The broader the chemical shift range, the higher the chemical shift dispersion. Additionally, the higher the standard deviation of the average chemical shift, the higher the chemical shift dispersion. For a given peptide, the chemical shift range was broader for the H $\alpha$  signals than for the HN signals (Table 1). Similarly, the standard deviation of the average chemical shift was higher for the H $\alpha$  signals than for the HN signals. The HN and H $\alpha$  chemical shift ranges followed the trend HPDFZbbXaa > HPDZbbXaa > HPDUZbbXaa, except for the HN chemical shift range for HPDAspDap versus HPDUAspDap (Table 1). Nonetheless, the H $\alpha$  chemical shift range for this exception followed the aforementioned general trend. The standard deviation of the average chemical shifts of the HN and H $\alpha$  protons followed the trend HPDFZbbXaa > HPDZbbXaa > HPDUZbbXaa, except for the standard deviation of the average HN chemical shifts for HPDAspDap versus HPDUAspDap (Table 1). Nevertheless, the standard deviation of the average H $\alpha$  chemical shift for this exception followed the aforementioned general trend. The exception in the HN chemical shift dispersion for HPDAspDap versus HPDUAspDap was most likely because the HN chemical shift is more sensitive to the neighboring residues in the primary sequence, whereas the H $\alpha$  chemical shift is more sensitive to the structural environment [45]. Accordingly, the HN chemical shift dispersion could be either higher than or similar to the H $\alpha$  chemical shift dispersion in the unfolded form, whereas the HN chemical shift dispersion could be lower than the H $\alpha$  chemical shift dispersion in the folded form [45], thereby resulting in the exception in the HN chemical shift dispersion for HPDAspDap versus HPDUAspDap. Overall, the chemical shift dispersion of peptides with a given Zbb2-Xaa9 pair followed the trend HPDFZbbXaa > HPDZbbXaa > HPDUZbbXaa (Tables 1 and S1–S36). Since the higher the chemical shift dispersion, the higher the folded population [45], these results were consistent with the intended designs.

**Table 1.** The chemical shift range and average chemical shift of the  $\delta$ HN and  $\delta$ H $\alpha$  for the HPDFZbbXaa, HPDZbbXaa, and HPDUZbbXaa peptides.

Peptide	$\delta$ HN Range <sup>1</sup> (ppm)	Average $\delta$ HN (ppm)	$\delta$ H $\alpha$ Range <sup>1</sup> (ppm)	Average $\delta$ H $\alpha$ (ppm)
HPDFAspDap	1.145	8.697 $\pm$ 0.336	1.428	4.664 $\pm$ 0.426
HPDAspDap	0.728	8.406 $\pm$ 0.195	1.009	4.374 $\pm$ 0.276
HPDUAspDap	0.769	8.366 $\pm$ 0.196	0.782	4.351 $\pm$ 0.209
HPDFAspDab	1.169	8.662 $\pm$ 0.339	1.407	4.649 $\pm$ 0.406
HPDAspDab	0.665	8.386 $\pm$ 0.171	0.902	4.368 $\pm$ 0.265
HPDUAspDab	0.570	8.378 $\pm$ 0.153	0.693	4.318 $\pm$ 0.177
HPDFAspOrn	1.124	8.637 $\pm$ 0.333	1.397	4.622 $\pm$ 0.391
HPDAspOrn	0.530	8.346 $\pm$ 0.150	0.895	4.338 $\pm$ 0.250
HPDUAspOrn	0.429	8.317 $\pm$ 0.133	0.723	4.279 $\pm$ 0.193
HPDFAspLys	1.108	8.625 $\pm$ 0.329	1.373	4.608 $\pm$ 0.384
HPDAspLys	0.454	8.326 $\pm$ 0.135	0.878	4.328 $\pm$ 0.244
HPDUAspLys	0.432	8.302 $\pm$ 0.127	0.718	4.276 $\pm$ 0.192
HPDFGluDap	1.119	8.740 $\pm$ 0.330	1.506	4.673 $\pm$ 0.421
HPDGluDap	0.795	8.482 $\pm$ 0.206	1.135	4.404 $\pm$ 0.294
HPDUGluDap	0.574	8.398 $\pm$ 0.172	0.772	4.326 $\pm$ 0.187
HPDFGluDab	1.192	8.706 $\pm$ 0.337	1.467	4.653 $\pm$ 0.404
HPDGluDab	0.626	8.417 $\pm$ 0.179	1.008	4.398 $\pm$ 0.278
HPDUGluDab	0.373	8.368 $\pm$ 0.126	0.514	4.299 $\pm$ 0.148
HPDFGluOrn	1.166	8.695 $\pm$ 0.343	1.457	4.640 $\pm$ 0.394
HPDGluOrn	0.584	8.427 $\pm$ 0.176	0.977	4.369 $\pm$ 0.258
HPDUGluOrn	0.324	8.348 $\pm$ 0.106	0.494	4.289 $\pm$ 0.140
HPDFGluLys	1.217	8.686 $\pm$ 0.360	1.452	4.630 $\pm$ 0.390

Table 1. Cont.

Peptide	$\delta\text{HN}$ Range <sup>1</sup> (ppm)	Average $\delta\text{HN}$ (ppm)	$\delta\text{H}\alpha$ Range <sup>1</sup> (ppm)	Average $\delta\text{H}\alpha$ (ppm)
HPDGluLys	0.618	8.427 ± 0.179	0.959	4.395 ± 0.237
HPDUGluLys	0.355	8.350 ± 0.102	0.584	4.278 ± 0.165
HPDFAadDap	1.135	8.738 ± 0.335	1.536	4.681 ± 0.424
HPDAadDap	0.793	8.476 ± 0.211	1.140	4.410 ± 0.296
HPDUAadDap	0.587	8.298 ± 0.169	0.782	4.244 ± 0.190
HPDFAadDab	1.183	8.702 ± 0.344	1.458	4.654 ± 0.402
HPDAadDab	0.675	8.445 ± 0.192	0.958	4.390 ± 0.268
HPDUAadDab	0.367	8.355 ± 0.116	0.515	4.300 ± 0.148
HPDFAadOrn	1.182	8.693 ± 0.340	1.442	4.638 ± 0.390
HPDAadOrn	0.535	8.405 ± 0.164	0.906	4.359 ± 0.247
HPDUAadOrn	0.273	8.333 ± 0.092	0.513	4.261 ± 0.163
HPDFAadLys	1.207	8.687 ± 0.357	1.455	4.629 ± 0.387
HPDAadLys	0.599	8.399 ± 0.172	0.927	4.360 ± 0.249
HPDUAadLys	0.276	8.317 ± 0.084	0.530	4.255 ± 0.165

<sup>1</sup> The chemical shift range was the difference between the chemical shift of the most downfield signal and the chemical shift of the most upfield signal for the proton of interest.

The  $\beta$ -hairpin structure of the peptides was confirmed by the chemical shift deviation of the  $\text{H}\alpha$  signals,  $^3J_{\text{NH}\alpha}$  spin–spin coupling constants, and cross-strand NOE signals. The  $\text{H}\alpha$  chemical shift deviation ( $\Delta\delta\text{H}\alpha$ ) is the difference between the  $\text{H}\alpha$  signal of the residue of interest and the corresponding  $\text{H}\alpha$  signal of the residue in the random coil conformation. The fully unfolded reference peptides were assumed to be random coil in this study [3,19,25–27,37]. A positive  $\Delta\delta\text{H}\alpha$  value represents an extended  $\beta$ -sheet conformation [46,47]. Residues Zbb2 through Val5 and Orn8 through Leu11 showed positive  $\Delta\delta\text{H}\alpha$  values for all of the experimental HPDZbbXaa peptides and all the fully folded reference HPDFZbbXaa peptides (Figures 2, S1 and S2), consistent with an extended  $\beta$ -strand conformation for these strand residues. The  $\Delta\delta\text{H}\alpha$  values of terminal residues Arg1 and Gln12 for the experimental peptides were close to zero (Figures 2b and S1), most likely resulting from the end fraying effect [3,23,25–27]. The  $\Delta\delta\text{H}\alpha$  values of Gly7 were negative or close to zero for all peptides, consistent with a turn conformation for Gly7 [43]. In general, residues in the strand regions (residues 2–5 and 8–11) showed more positive  $\Delta\delta\text{H}\alpha$  values for the fully folded reference peptides, compared to those in the corresponding experimental peptides, suggesting that the fully folded reference peptides exhibited a higher  $\beta$ -hairpin population than the corresponding experimental peptides. This was consistent with the intended designs.

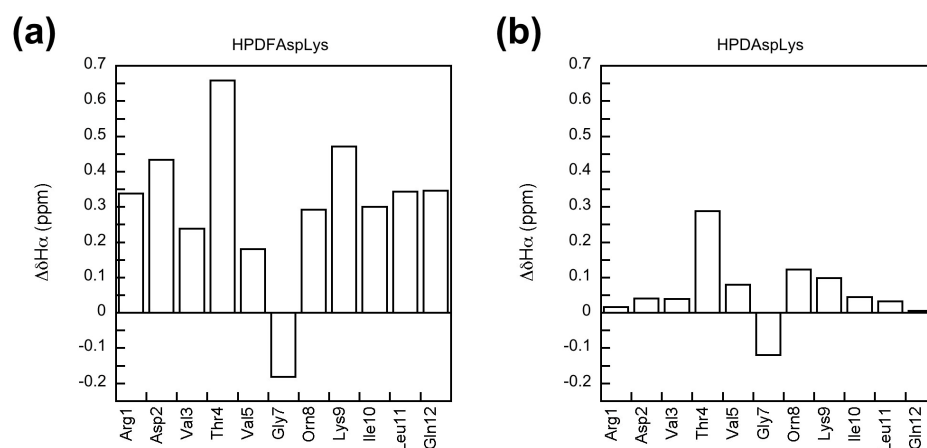


Figure 2. The chemical shift deviation ( $\Delta\delta\text{H}\alpha$ ) for the residues in peptides HPDFAspLys (a) and HPDAspLys (b).

The  $^3J_{NH\alpha}$  spin–spin coupling constants for each residue in the peptides were determined using the DQF-COSY spectra (Tables S37–S45) [48]. The  $^3J_{NH\alpha}$  values for the strand residues in the experimental HPDZbbXaa peptides were higher than 7 Hz (Tables S37–S39), suggesting a  $\beta$ -conformation [42,49]. The  $^3J_{NH\alpha}$  values for the strand residues in the fully folded reference HPDFZbbXaa peptides were also higher than 7 Hz, and most of the values were higher than those for the corresponding residues in the experimental HPDZbbXaa peptides (Tables 2 and S37–S42). This suggested that the fully folded reference HPDFZbbXaa peptides were more folded than the corresponding experimental HPDZbbXaa peptides. If one disregards the standard deviations, most of the average  $^3J_{NH\alpha}$  values followed the trend HPDFZbbXaa > HPDZbbXaa > HPDUZbbXaa (Table 2). Overall, these trends were consistent with the intended designs.

**Table 2.** The average  $^3J_{NH\alpha}$  coupling constant values for the strand residues in the HPDFZbbXaa, HPDZbbXaa, and HPDUZbbXaa peptides <sup>1</sup>.

Zbb	Xaa	HPDFZbbXaa	HPDZbbXaa	HPDUZbbXaa
Asp	Dap	11 ± 0.7	9.8 ± 1.0	10 ± 1.2
Asp	Dab	11 ± 1.6	9.4 ± 1.5	8.3 ± 2.2
Asp	Orn	12 ± 0.7	10 ± 1.0	9.7 ± 0.8
Asp	Lys	12 ± 0.6	10 ± 0.8	10 ± 1.0
Glu	Dap	10 ± 0.9	9.9 ± 0.9	9.6 ± 1.3
Glu	Dab	10 ± 1.1	9.5 ± 2.1	9.2 ± 1.6
Glu	Orn	11 ± 0.6	10 ± 0.6	10 ± 0.6
Glu	Lys	11 ± 1.1	9.6 ± 0.9	9.2 ± 1.0
Aad	Dap	11 ± 0.9	9.7 ± 1.4	9.9 ± 1.0
Aad	Dab	10 ± 1.0	9.4 ± 1.7	9.8 ± 1.0
Aad	Orn	12 ± 0.7	10 ± 0.7	9.3 ± 0.5
Aad	Lys	11 ± 0.5	9.9 ± 0.5	9.6 ± 0.7

<sup>1</sup> The average  $^3J_{NH\alpha}$  coupling constant values for the strand residues were calculated without including values for Gly, which is in the  $\beta$ -turn.

All cross-peaks in the ROESY spectra were assigned. Intra-residue, sequential, medium-range, and long-range NOEs (Figures S3–S50) with a number of cross-strand H $\alpha$ -to-H $\alpha$ , H $\alpha$ -to-NH, NH-to-NH correlations were observed in the ROESY spectra (Figures S39–S50). Strong sequential H $\alpha_i$ -NH $_{i+1}$  correlations were observed for every strand on all peptides, suggesting an extended  $\beta$ -strand conformation (Figures S39–S50). The cross-strand NOE connectivities obtained from the ROESY spectra further supported the intended  $\beta$ -hairpin conformation for the fully folded reference HPDFZbbXaa peptides and the experimental HPDZbbXaa peptides (Figures S3–S38). For a given Zbb2-Xaa9 combination, the number of cross-strand NOE connectivities (including both side-chain and backbone) followed the trend HPDFZbbXaa > HPDZbbXaa > HPDUZbbXaa (Figures S3–S50). Since more cross-strand NOE connectivities should correspond to a higher fraction  $\beta$ -hairpin structure, these trends are consistent with the intended designs.

### 2.3. Fraction Folded Population and Folding Free Energy

The fraction folded population and folding free energy ( $\Delta G_{\text{fold}}$ ) for each residue on the experimental HPDZbbXaa peptides were derived from the H $\alpha$  chemical shift data (Figures S51 and S52). The ratio of the chemical shift deviation ( $\Delta\delta H\alpha$ ) for a given residue on the experimental HPDZbbXaa peptide to the corresponding value on the fully folded reference HPDFZbbXaa peptide gave the fraction folded population for the residue of interest in the experimental peptide (Figure S51) [3,19,25–27,37]. The average of the fraction folded population for residues at positions 2, 3, 9, and 10 was used to represent the fraction folded population of the corresponding peptide (Table 3) [3,25–27]. These residues were not at the termini of the peptide, at which residues suffered from end fraying effects, nor were these residues adjacent to the turn, at which residues exhibited intrinsically higher fraction folded population [3,19,23,25–27]. Furthermore, both strands, and both hydrogen and

non-hydrogen bonded positions, were equally represented in the chosen residues [3,25–27]. Similarly, the average of the  $\Delta G_{\text{fold}}$  for residues at positions 2, 3, 9, and 10 was used to represent the  $\Delta G_{\text{fold}}$  of the corresponding peptide (Table 4) [3,25–27]. Since the  $\Delta G_{\text{fold}}$  exhibited the same trends as the fraction folded population (i.e., the higher the fraction folded population, the less positive the  $\Delta G_{\text{fold}}$ ), only the fraction folded population data are discussed in detail.

**Table 3.** The fraction folded population (%) for HPDZbbXaa peptides <sup>1</sup>.

Xaa9	Zbb2		
	Asp	Glu	Aad
Dap	19 ± 4	38 ± 4	47 ± 4
Dab	25 ± 4	42 ± 3	40 ± 3
Orn	17 ± 4	36 ± 3	33 ± 3
Lys	15 ± 5	36 ± 4	36 ± 3

<sup>1</sup> Average value for residues 2, 3, 9, and 10.

**Table 4.** The folding free energy ( $\Delta G_{\text{fold}}$ , kcal/mol) for HPDZbbXaa peptides <sup>1</sup>.

Xaa9	Zbb2		
	Asp	Glu	Aad
Dap	0.864 ± 0.177	0.303 ± 0.091	0.062 ± 0.085
Dab	0.665 ± 0.143	0.185 ± 0.065	0.231 ± 0.070
Orn	0.975 ± 0.188	0.347 ± 0.075	0.424 ± 0.077
Lys	1.031 ± 0.231	0.333 ± 0.107	0.345 ± 0.086

<sup>1</sup> Average value for residues 2, 3, 9, and 10.

The fraction folded population for HPDZbbXaa peptides was between 15% and 47% with standard deviations within 5% (Table 3). HPDAadDap exhibited the highest fraction folded population among all HPDZbbXaa peptides. HPDAspLys exhibited the least fraction folded population among the peptides. If one disregards HPDAspDap, the fraction folded population of HPDZbbXaa peptides with a given negatively charged residue Zbb2 generally decreased as the side-chain length of the positively charged residue Xaa9 increased. Furthermore, the fraction folded population of HPDZbbXaa peptides with a given positively charged residue Xaa9 generally increased as the side-chain length of the negatively charged residues Zbb2 increased from Asp to Glu but mostly remained similar upon increasing Glu to Aad.

#### 2.4. Diagonal Cross-Strand Zbb-Xaa Interactions

The interaction free energy ( $\Delta G_{\text{int}}$ ) for each potential diagonal Zbb2-Xaa9 interaction was derived by double mutant cycle analysis (Table 5) [50]. The double mutant cycle was used to remove the inherent effect of individually incorporating the charged residues Zbb2 and Xaa9 from the effect of simultaneously incorporating both Zbb2 and Xaa9 [25–27]. The energy difference between the  $\Delta G_{\text{fold}}$  of HPDZbbXaa and HPDAlaAla represented the effect of simultaneously incorporating both Zbb2 and Xaa9. The energy difference between the  $\Delta G_{\text{fold}}$  of HPDZbbAla (and HPDAlaXaa) and HPDAlaAla represented the effect of individually incorporating Zbb2 (and Xaa9) on  $\beta$ -hairpin stability. The Zbb2-Xaa9 interaction energy ( $\Delta G_{\text{int}}$ ) was derived from the folding free energy for the peptides HPDZbbXaa, HPDZbbAla [38], HPDAlaXaa [38], and HPDAlaAla (Table 5).

**Table 5.** The diagonal Zbb2-Xaa9 ion-pairing interaction energy ( $\Delta G_{\text{int}}$ , kcal/mol).

Xaa9	Zbb2		
	Asp	Glu	Aad
Dap	$-0.434 \pm 0.204$	$-0.412 \pm 0.043$	$-0.425 \pm 0.077$
Dab	$-0.794 \pm 0.139$	$-0.585 \pm 0.058$	$-0.284 \pm 0.030$
Orn	$-0.375 \pm 0.081$	$-0.291 \pm 0.048$	$-0.023 \pm 0.040$
Lys	$-0.206 \pm 0.018$	$-0.258 \pm 0.026$	$-0.020 \pm 0.045$

Most of the cross-strand diagonal Zbb2-Xaa9 interactions were apparently stabilizing (Table 5). However, there was no apparent Aad2-Orn9 or Aad2-Lys9 interaction. Nonetheless, the Asp2-Dab9 interaction was the most stabilizing, providing up to  $-0.794$  kcal/mol stabilization. The Zbb2-Dap9 interactions were similar in energy regardless of the negatively charged Zbb2 residue. For the HPDZbbDab and HPDZbbOrn peptides, the  $\Delta G_{\text{int}}$  for the Zbb2-Dab9 and Zbb2-Orn9 interactions followed the trend Asp < Glu < Aad. For the HPDZbbLys peptides, the  $\Delta G_{\text{int}}$  for the Zbb2-Lys9 interaction followed the trend Asp > Glu < Aad. If one disregards the Asp2-Dap9 and Glu2-Dap9 interactions, the  $\Delta G_{\text{int}}$  for the Zbb2-Xaa9 interaction was less stabilizing upon increasing the Xaa9 side-chain length for a given negatively charged Zbb2 residue.

### 3. Discussion

The effects of side-chain length on diagonal ion-pairing interactions between carboxylate- and ammonium-containing residues in a  $\beta$ -hairpin was investigated. The fraction folded population for the experimental HPDZbbXaa peptides was 15–47% (Table 3). The variation in the fraction folded population of HPDZbbXaa peptides can be rationalized by the intrinsic sheet propensity of the carboxylate- and ammonium-containing amino acids with different side-chain lengths at positions 2 and 9, respectively, and the potential cross-strand diagonal Zbb2-Xaa9 ion-pairing interaction. In general, the fraction folded population for the HPDZbbXaa peptides with a given positively charged residue Xaa9 increased as the side-chain length of the negatively charged residues Zbb2 increased from Asp to Glu but mostly remained similar upon increasing Glu to Aad (Table 3). This trend is similar to the fraction folded population trend for the the HPDZbbAla peptides (with the negatively charged residue Zbb at position 2 and Ala at position 9) [38], suggesting that there may be small variations in the diagonal Zbb2-Xaa9 interactions in the HPDZbbXaa peptides. However, the fraction folded population for the HPDZbbXaa peptides with a given negatively charged residue Zbb2 generally decreased as the side-chain length of the positively charged residue Xaa9 increased (Table 3). This trend is opposite of the fraction folded population trend for the HPDAAlaXaa peptides (with Ala at position 2 and the positively charged ammonium-containing residue Xaa at position 9) [38], suggesting variation in the diagonal Zbb2-Xaa9 interaction in the HPDZbbXaa peptides. Indeed, the diagonal Zbb2-Xaa9 interaction varied with side-chain length combination (Table 5).

How do the HPDZbbXaa peptides with a diagonal Zbb2-Xaa9 interaction measure up to the HPTZbbXaa peptides with a lateral Zbb4-Xaa9 interaction [25]? The constituting amino acids for the two sets of peptides were the same, but Thr and Zbb were incorporated at positions 2 and 4, respectively, in the HPTZbbXaa peptides [25]. The fraction folded population of the HPDZbbXaa peptides was mostly lower than that of the corresponding HPTZbbXaa peptides [25], except for HPDGluDab, HPDAadDap, and HPDAadDab. Furthermore, the range for the fraction folded population of the HPDZbbXaa peptides was narrower than that of the HPTZbbXaa peptides (24–63%) [25]. The HPDAadDap ( $47 \pm 4\%$ ) and HPDGluDab ( $42 \pm 3\%$ ) peptides exhibited the highest fraction folded populations for the HPDZbbXaa peptides in this study. Surprisingly, HPTAadDap ( $25 \pm 1\%$ ) and HPTGluDab ( $24 \pm 2\%$ ) exhibited the lowest fraction folded populations for the HPTZbbXaa peptides [25]. These differences may be due to the effect of incorporating the negatively charged residue at position 2 versus 4, the effect of incorporating Thr at

position 4 versus 2, and the difference in the diagonal Zbb2-Xaa9 interaction and the lateral Zbb4-Xaa9 interaction. The fraction folded populations of HPDAspAla ( $8 \pm 5\%$ ) and HPDGluAla ( $19 \pm 5\%$ ) were lower than those of HPTAspAla ( $37 \pm 1\%$ ) and HPTGluAla ( $29 \pm 2\%$ ) [3,38], respectively, whereas the fraction folded populations of HPDAadAla ( $26 \pm 4\%$ ) and HPTAadAla ( $25 \pm 2\%$ ) were essentially the same [3,38]. Furthermore, the fraction folded populations for HPDAlaDab ( $21 \pm 3\%$ ) and HPDAlaLys ( $27 \pm 3\%$ ) were higher than those for HPTAlaDab ( $14 \pm 3\%$ ) and HPTAlaLys ( $22 \pm 3\%$ ) [3,38], respectively, whereas the fraction folded populations of HPDAlaDap ( $19 \pm 6\%$ ) and HPDAlaOrn ( $24 \pm 3\%$ ) were similar to those of HPTAlaDap ( $16 \pm 1\%$ ) and HPTAlaOrn ( $21 \pm 3\%$ ) [3,38], respectively. Both HPDAadDap and HPDGluDab exhibited relatively high fraction folded populations, most likely because the relatively longer Aad and Glu side chains favor strand formation [38], coupled with reasonably stabilizing diagonal Aad2-Dap9 and Glu2-Dab9 ion-pairing interaction (Table 5), respectively.

The diagonal ion-pairing interaction between carboxylate- and ammonium-containing residues with varying side-chain lengths provided up to 0.79 kcal/mol stabilization in  $\beta$ -hairpins (Table 5). This is on par with the diagonal hydrophobics/ $\pi$ -related interactions, which provided up to 1.0 kcal/mol stabilization in  $\beta$ -hairpins [24,29–35]. Furthermore, the diagonal ion-pairing interaction in this study also matched the analogous lateral ion-pairing interaction, which provided up to 0.83 kcal/mol stabilization in  $\beta$ -hairpins [25]. Focusing on the encoded amino acids, the diagonal Asp2-Lys9 ( $-0.21$  kcal/mol) and Glu2-Lys9 ( $-0.26$  kcal/mol) interactions were more stabilizing than the lateral Asp4-Lys9 ( $-0.11$  kcal/mol), Glu4-Lys9 ( $-0.02$  kcal/mol), Lys4-Asp9 (destabilizing), and Lys4-Glu9 (destabilizing) interactions [3,27]. The diagonal Asp2-Dab9 and Glu2-Dab9 interactions were the most stabilizing among the diagonal Zbb2-Xaa9 pairs. However, the lateral Asp4-Dab9 and Glu4-Dab9 pairs showed no apparent interaction in our previous study [25]. This may be due to the difference in the relative positioning of the potentially interacting residues for the diagonal and lateral interactions. Based on the solution structure of an analogue of the parent YKL peptide [51], the C $\alpha$ -C $\alpha$  distance for the diagonal Zbb2-Xaa9 pair is 5.91 Å (591 pm), whereas the C $\alpha$ -C $\alpha$  distance for the lateral Zbb4-Xaa9 pair is 3.96 Å (396 pm). Furthermore, the C $\beta$ -C $\beta$  distance for the diagonal Zbb2-Xaa9 pair is 4.85 Å (485 pm), whereas the C $\beta$ -C $\beta$  distance for the lateral Zbb4-Xaa9 pair is 5.41 Å (541 pm). According to this solution structure [51], diagonal pairs point toward each other, whereas lateral pairs point away from each other (Figure 3).

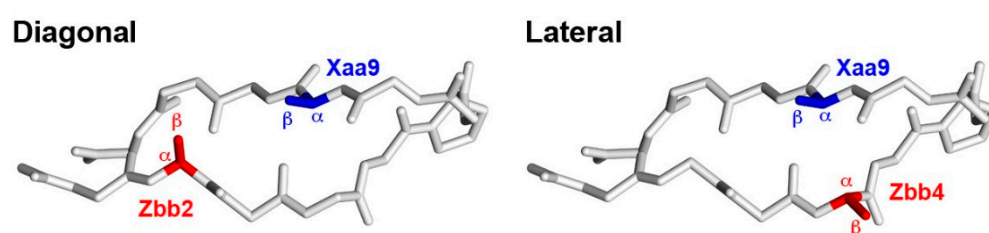


**Figure 3.** The backbone of the solution structure of an analogue of the parent YKL peptide (pdb code 1JY9 [51]) along with the intended diagonal (**left**) and lateral (**right**) interacting residues. The backbone and DPro side chains are shown in white. The C $\alpha$  and C $\beta$  of the negatively charged residues are shown in red, and C $\alpha$  and C $\beta$  of the positively charged residues are shown in blue.

The  $\Delta G_{\text{int}}$  for the diagonal Zbb2-Dap9 interactions were similar regardless of the negatively charged Zbb2 side-chain length. The Asp2-Dap9 ion pair should suffer the least side-chain conformational entropic penalty for ion pair formation, compared to the other Zbb2-Dap9 ion-pairs, because the Asp side-chain length is the shortest among the carboxylate-containing residues. Increasing the carboxylate-containing Zbb2 side-chain length would increase the side-chain conformational entropic penalty for the Zbb2-Dap9 ion-pair formation but would also increase the number of side-chain conformations that could accommodate a Zbb2-Dap9 ion-pair to compensate for the increased entropic penalty for ion-pair formation, resulting in similar  $\Delta G_{\text{int}}$  values. Increasing the Dap side-chain

length in the Asp2-Dap9 ion-pair to the Asp2-Dab9 ion pair resulted in the most stabilizing diagonal ion-pairing interaction, suggesting that the increase in the number of side-chain conformations that could accommodate an Asp2-Dab9 ion-pair outweighed the increase in the side-chain conformational entropic penalty for ion-pair formation upon lengthening Dap9 to Dab9. Further side-chain lengthening of either Asp2 or Dab9 (or both) resulted in a drop in stabilization for the Zbb2-Xaa9 interaction, suggesting that the increase in the number of conformations that could accommodate a Zbb2-Xaa9 ion-pair could no longer compensate for the increase in the entropic penalty for ion-pair formation. As such, the diagonal Asp2-Dab9 ion-pairing interaction most likely represents an optimal balance between side-chain conformational entropic penalty and the number of side-chain conformations to support the Asp2-Dab9 interaction. This is in sharp contrast to the length matching requirements for the lateral Zbb4-Xaa9 interaction [25], in which the longer side chains most likely interact through hydrophobics and the shorter side chains most likely interact through electrostatics.

#### 4. Materials and Methods

##### 4.1. Peptide Synthesis and Purification

Peptides were synthesized by solid-phase peptide synthesis using Fmoc-based chemistry [39,40]. The disulfide bond in the HPDFZbbXaa peptides was formed via charcoal-mediated air oxidation [41]. All peptides were purified by reverse-phase high-performance liquid chromatography (RP-HPLC) to higher than 95% purity (except for HPDAspDap, HPDAspDab, HPDGluDap, HPDGluDab, and HPDAadDab, which were purified to higher than 90% purity). The identity of the peptides was confirmed by matrix-assisted laser desorption ionization time-of-flight mass spectroscopy (MALDI-TOF). More detailed procedures and peptide characterization data are provided in the Supplementary Materials.

##### 4.2. Chemical Shift Deviation

Purified peptides were dissolved in a H<sub>2</sub>O/D<sub>2</sub>O (9:1 ratio by volume) in the presence of 50 mM sodium deuterioacetate buffer (pH 5.5, uncorrected) to give peptide concentrations of 0.9–10.1 mM. 2-Dimethyl-2-silapentane-5-sulfonate was added to the sample as an internal reference. All NMR experiments were performed on a Brüker AV III 800 MHz spectrometer. Phase-sensitive total correlation spectroscopy (TOCSY) [52], rotating-frame nuclear Overhauser effect spectroscopy (ROESY) [53], and double-quantum filtered-correlated spectroscopy (DQF-COSY) [54] experiments were performed by collecting 2048 points in f<sub>2</sub> with 4–8 scans and 256–512 points in f<sub>1</sub> at 298 K. Solvent suppression was achieved by the WATERGATE solvent suppression sequence [55]. TOCSY and ROESY experiments employed a spin locking field of 10 kHz. Mixing times of 60 and 200 ms were used for the TOCSY and ROESY experiments, respectively.

##### 4.3. Nuclear Magnetic Resonance Spectroscopy

Sequence-specific assignments for all peptides were completed by using the 2D-NMR spectra (TOCSY and ROESY). The chemical shift deviation ( $\Delta\delta H\alpha$ ) for each residue of the experimental peptide ( $\Delta\delta H\alpha(\text{exp})$ ) and the folded reference peptide ( $\Delta\delta H\alpha(\text{F})$ ) was derived using Equations (1) and (2), respectively [46].  $\delta H\alpha(\text{exp})$  is the chemical shift for the residue of interest on the experimental peptide.  $\delta H\alpha(\text{U})$  is the chemical shift for the corresponding residue of interest on the fully unfolded reference peptide.  $\delta H\alpha(\text{F})$  is the chemical shift for the corresponding residue of interest on the fully folded reference peptide.

$$\Delta\delta H\alpha(\text{exp}) = \delta H\alpha(\text{exp}) - \delta H\alpha(\text{U}) \quad (1)$$

$$\Delta\delta H\alpha(\text{F}) = \delta H\alpha(\text{F}) - \delta H\alpha(\text{U}) \quad (2)$$

#### 4.4. ${}^3J_{NH\alpha}$ Spin–Spin Coupling Constant

The peak-to-peak separation in the absorptive ( $\nu_a$ ) and dispersive ( $\nu_d$ ) DQF-COSY spectra was measured to derive the  ${}^3J_{NH\alpha}$  coupling constant using the values along the f2 axis. The absorptive ( $\nu_a$ ) and dispersive ( $\nu_d$ ) values were used to derive the coupling constants from the square root of the single real root using Equation (3) [48].

$$J^6 - \nu_a^2 J^4 + \left( -\frac{9}{4}\nu_a^4 + \frac{3}{2}\nu_a^2\nu_d^2 + \frac{3}{4}\nu_d^4 \right) J^2 + \frac{81}{64}\nu_a^6 - \frac{9}{16}\nu_a^4\nu_d^2 - \frac{21}{32}\nu_a^2\nu_d^4 - \frac{1}{16}\nu_d^6 - \frac{\nu_d^8}{64\nu_a^2} = 0 \quad (3)$$

#### 4.5. Interproton Distance Determination via NOE Integration

The NOE cross-peaks of all peptides were assigned from the corresponding ROESY spectra. Integration was performed based on a Gaussian peak model to obtain the intensity of cross-peaks. The distance between the two  $\beta$ -hydrogen atoms on the proline side chain (1.77 Å) was set as the standard to derive the interproton distance for the cross-peak of interest using Equation (4). The distances were grouped into short ( $\leq 2.5$  Å), medium (2.5–3.5 Å), and long ( $> 3.5$  Å) for the illustrations in the Wüthrich diagrams (Figures S39–S50).

$$R_{\text{residue}} = 1.77 \times 10^{-10} \times \left( \frac{I_{\text{standard}}}{I_{\text{residue}}} \right)^{\frac{1}{6}} \quad (4)$$

#### 4.6. Fraction Folded Population and Folding Free Energy ( $\Delta G_{\text{fold}}$ )

The equilibrium constant between the unfolded and folded states of an experimental peptide is the ratio of the folded and unfolded populations. The fraction folded population for each residue was derived from the chemical shift data using Equation (5). The folding free energy  $\Delta G_{\text{fold}}$  for each residue was derived using Equation (6). The fraction folded populations and folding free energy ( $\Delta G_{\text{fold}}$ ) of peptides were obtained by averaging the corresponding values for residues at positions 2, 3, 9, and 10 [3,19,22,25–27,38]. These four positions were in the middle of the strands, neither at the termini (which would suffer from the end fraying effect) nor directly attached to the turn (which would promote sheet formation). Furthermore, the average value of these four positions would provide equal representation for both hydrogen-bonded positions (residues 3 and 10) and non-hydrogen-bonded positions (residues 2 and 9), and also equal representation for both strands in the hairpin (i.e., the N-terminal strand: residues 2 and 3; the C-terminal strand: residues 9 and 10).

$$\text{Fraction Folded Population} = \frac{\delta H\alpha(\text{exp}) - \delta H\alpha(\text{U})}{\delta H\alpha(\text{F}) - \delta H\alpha(\text{U})} \times 100\% \quad (5)$$

$$\Delta G_{\text{fold}} = -RT \ln \frac{\delta H\alpha(\text{exp}) - \delta H\alpha(\text{U})}{\delta H\alpha(\text{F}) - \delta H\alpha(\text{exp})} \quad (6)$$

#### 4.7. Double Mutant Cycle Analysis

Double mutant cycle analysis [50] was performed to determine the interaction free energy ( $\Delta G_{\text{int}}$ ) between charged residues Zbb2 and Xaa9 in HPDZbbXaa peptides using Equation (7). This analysis accounted for the effect of each charged residue (individually) on strand stability using data from the corresponding Ala-containing peptides HPDZbbAla and HPDAlaXaa [38] to determine the Zbb2-Xaa9 ion-pairing interaction exclusively. The peptide with Ala incorporated at positions 2 and 9, HPDAlaAla, was used as the reference peptide.

$$\Delta G_{\text{int}} = (\Delta G_{\text{HPDZbbXaa}} - \Delta G_{\text{HPDAlaAla}}) - (\Delta G_{\text{HPDZbbAla}} - \Delta G_{\text{HPDAlaAla}}) - (\Delta G_{\text{HPDAlaXaa}} - \Delta G_{\text{HPDAlaAla}}) \quad (7)$$

## 5. Conclusions

The effects of charged amino acid side-chain length on diagonal cross-strand ion-pairing interaction between carboxylate- and ammonium-containing residues was investigated in a  $\beta$ -hairpin by NMR methods. HPDAadDap exhibited the highest fraction folded population because the long Aad side chain inherently favors strand formation coupled with the reasonably stabilizing diagonal Aad2-Dap9 ion-pairing interaction. Furthermore, the diagonal Asp2-Dab9 ion-pairing interaction was the most stabilizing interaction, most likely representing an optimal balance between the side-chain conformational entropic penalty to enable the ion-pairing interaction and the number of side-chain conformations that can accommodate the interaction. These results should be useful for stabilizing  $\beta$ -sheet containing molecular entities for various applications.  $\beta$ -Strand containing motifs have been used for specific recognition of various biomolecules including ATP [56], DNA [57,58], and RNA [59–64]. Furthermore,  $\beta$ -sheet containing peptides have been developed for ion channel blocking [65], bacterial endotoxin inhibition [66], antimicrobial activity [67], hydrogel formation [68–75], and intracellular delivery [76,77]. The results in this study may also facilitate the design of  $\beta$ -strand containing molecules for reducing amyloid [78], or for inhibiting protein–protein interactions involving  $\beta$ -structures [79,80].

**Supplementary Materials:** The following are available online at <https://www.mdpi.com/article/10.3390/molecules27134172/s1>, Tables S1–S36: The  $^1\text{H}$  chemical shift assignments for the peptides, Tables S37–S45: The  $^3J_{\text{NH}\alpha}$  values of the peptides, Figure S1: The  $\text{H}\alpha$  chemical shift deviations for the residues in the experimental HPDZbbXaa peptides, Figure S2: The  $\text{H}\alpha$  chemical shift deviations for the residues in the fully folded reference HPDFZbbXaa peptides, Figures S3–S38: The NOEs observed involving the side chains of the peptides, Figures S39–S50: Wüthrich diagrams of the backbone NOE connectivities involving the  $\alpha$ -protons and amide protons for the peptides, Figure S51: The fraction folded of the residues in the peptides, Figure S52: The  $\Delta G_{\text{fold}}$  of the residues in the peptides.

**Author Contributions:** Conceptualization, R.P.C.; methodology, R.P.C.; software, Y.-J.P., P.-Y.H., Y.-T.S. and C.-H.Y.; validation, J.-Y.C., C.-H.Y. and Z.-J.N.; formal analysis, J.-Y.C., Y.-J.P., P.-Y.H., Y.-T.S. and C.-H.Y.; investigation, S.-J.H. and S.-L.H.; resources, Y.-J.P., P.-Y.H. and Y.-T.S.; data curation, J.-Y.C., Y.-J.P., P.-Y.H., Y.-T.S., C.-H.Y. and Z.-J.N.; writing—original draft preparation, J.-Y.C., Y.-J.P. and P.-Y.H.; writing—review and editing, J.-Y.C. and R.P.C.; visualization, J.-Y.C., Y.-J.P., P.-Y.H. and R.P.C.; supervision, R.P.C.; project administration, R.P.C.; funding acquisition, R.P.C. All authors have read and agreed to the published version of the manuscript.

**Funding:** This research was funded by the Ministry of Science and Technology in Taiwan, MOST-103-2113-M-002-018-MY3 and MOST-110-2113-M-002-010.

**Institutional Review Board Statement:** Not applicable.

**Informed Consent Statement:** Not applicable.

**Data Availability Statement:** The data presented in this study are available in the Supplementary Materials. The raw data are available on request from the corresponding author.

**Acknowledgments:** The authors would like to thank Hsiou-Ting Kuo, Po-Yi Wu, and Wei-Ming Wang for their assistance in acquiring the NMR data. The authors would also like to thank the mass spectrometry services from the National Taiwan University Consortia of Key Technologies.

**Conflicts of Interest:** The authors declare no conflict of interest.

**Sample Availability:** Samples of the compounds are not available from the authors.

## References

1. Chou, P.Y.; Fasman, G.D. Conformational parameters for amino acids in helical,  $\beta$ -sheet, and random coil regions calculated from proteins. *Biochemistry* **1974**, *13*, 211–222. [[CrossRef](#)] [[PubMed](#)]
2. Muñoz, V.; Serrano, L. Intrinsic secondary structure propensities of the amino acids, using statistical  $\phi$ - $\psi$  matrices: Comparison with experimental scales. *Proteins* **1994**, *20*, 301–311. [[CrossRef](#)] [[PubMed](#)]
3. Kuo, L.-H.; Li, J.-H.; Kuo, H.-T.; Hung, C.-Y.; Tsai, H.-Y.; Chiu, W.-C.; Wu, C.-H.; Wang, W.-R.; Yang, P.-A.; Yao, Y.-C.; et al. Effect of Charged Amino Acid Side Chain Length at Non-Hydrogen Bonded Strand Positions on  $\beta$ -Hairpin Stability. *Biochemistry* **2013**, *52*, 7785–7797. [[CrossRef](#)] [[PubMed](#)]
4. Hardy, J.; Allsop, D. Amyloid deposition as the central event in the aetiology of Alzheimer's disease. *Trends Pharmacol. Sci.* **1991**, *12*, 383–388. [[CrossRef](#)]
5. Bartzokis, G.; Lu, P.H.; Mintz, J. Human brain myelination and amyloid beta deposition in Alzheimer's disease. *Alzheimers Dement.* **2007**, *3*, 122–125. [[CrossRef](#)]
6. Scherzinger, E.; Lurz, R.; Turmaine, M.; Mangiarini, L.; Hollenbach, B.; Hasenbank, R.; Bates, G.P.; Davies, S.W.; Lehrach, H.; Wanker, E.E. Huntingtin-Encoded Polyglutamine Expansions Form Amyloid-like Protein Aggregates In Vitro and In Vivo. *Cell* **1997**, *90*, 549–558. [[CrossRef](#)]
7. Truant, R.; Atwal, R.S.; Desmond, C.; Munsie, L.; Tran, T. Huntington's disease: Revisiting the aggregation hypothesis in polyglutamine neurodegenerative diseases. *FEBS J.* **2008**, *275*, 4252–4262. [[CrossRef](#)]
8. Irvine, G.B.; El-Agnaf, O.M.; Shankar, G.M.; Walsh, D.M. Protein Aggregation in the Brain: The Molecular Basis for Alzheimer's and Parkinson's Diseases. *Mol. Med.* **2008**, *14*, 451–464. [[CrossRef](#)]
9. Minor, D.L., Jr.; Kim, P.S. Measurement of the  $\beta$ -sheet-forming propensities of amino acids. *Nature* **1994**, *367*, 660–663. [[CrossRef](#)]
10. Smith, C.K.; Withka, J.M.; Regan, L. A thermodynamic scale for the  $\beta$ -sheet forming tendencies of the amino acids. *Biochemistry* **1994**, *33*, 5510–5517. [[CrossRef](#)]
11. Wouters, M.A.; Curmi, P.M.G. An analysis of side chain interactions and pair correlations within antiparallel  $\beta$ -sheets: The differences between backbone hydrogen-bonded and non-hydrogen-bonded residue pairs. *Proteins* **1995**, *22*, 119–131. [[CrossRef](#)]
12. Cootes, A.P.; Curmi, P.M.; Cunningham, R.; Donnelly, C.; Torda, A.E. The dependence of amino acid pair correlations on structural environment. *Proteins* **1998**, *32*, 175–189. [[CrossRef](#)]
13. Hutchinson, E.G.; Sessions, R.B.; Thornton, J.M.; Woolfson, D.N. Determinants of strand register in antiparallel  $\beta$ -sheets of proteins. *Protein Sci.* **1998**, *7*, 2287–2300. [[CrossRef](#)]
14. Smith, C.K.; Regan, L. Guidelines for Protein Design: The Energetics of  $\beta$  Sheet Side Chain Interactions. *Science* **1995**, *270*, 980–982. [[CrossRef](#)]
15. Merkel, J.S.; Sturtevant, J.M.; Regan, L. Sidechain interactions in parallel  $\beta$  sheets: The energetics of cross-strand pairings. *Structure* **1999**, *7*, 1333–1343. [[CrossRef](#)]
16. Blasie, C.A.; Berg, J.M. Electrostatic Interactions across a  $\beta$ -Sheet. *Biochemistry* **1997**, *36*, 6218–6222. [[CrossRef](#)]
17. Searle, M.S.; Griffiths-Jones, S.R.; Skinner-Smith, H. Energetics of Weak Interactions in a  $\beta$ -hairpin Peptide: Electrostatic and Hydrophobic Contributions to Stability from Lysine Salt Bridges. *J. Am. Chem. Soc.* **1999**, *121*, 11615–11620. [[CrossRef](#)]
18. Russell, S.J.; Cochran, A.G. Designing Stable  $\beta$ -Hairpins: Energetic Contributions from Cross-Strand Residues. *J. Am. Chem. Soc.* **2000**, *122*, 12600–12601. [[CrossRef](#)]
19. Syud, F.A.; Stanger, H.E.; Gellman, S.H. Interstrand Side Chain–Side Chain Interactions in a Designed  $\beta$ -Hairpin: Significance of Both Lateral and Diagonal Pairings. *J. Am. Chem. Soc.* **2001**, *123*, 8667–8677. [[CrossRef](#)]
20. Ramírez-Alvarado, M.; Blanco, F.J.; Serrano, L. Elongation of the BH8  $\beta$ -hairpin peptide: Electrostatic interactions in  $\beta$ -hairpin formation and stability. *Protein Sci.* **2001**, *10*, 1381–1392. [[CrossRef](#)]
21. Tatko, C.D.; Waters, M.L. Selective Aromatic Interactions in  $\beta$ -Hairpin Peptides. *J. Am. Chem. Soc.* **2002**, *124*, 9372–9373. [[CrossRef](#)]
22. Kiehna, S.E.; Waters, M.L. Sequence dependence of  $\beta$ -hairpin structure: Comparison of a salt bridge and an aromatic interaction. *Protein Sci.* **2003**, *12*, 2657–2667. [[CrossRef](#)]
23. Ciani, B.; Jourdan, M.; Searle, M.S. Stabilization of  $\beta$ -Hairpin Peptides by Salt Bridges: Role of Preorganization in the Energetic Contribution of Weak Interactions. *J. Am. Chem. Soc.* **2003**, *125*, 9038–9047. [[CrossRef](#)]
24. Tatko, C.D.; Waters, M.L. Comparison of C-H... $\pi$  and hydrophobic interactions in a  $\beta$ -hairpin peptide: Impact on stability and specificity. *J. Am. Chem. Soc.* **2004**, *126*, 2028–2034. [[CrossRef](#)] [[PubMed](#)]
25. Kuo, H.-T.; Fang, C.-J.; Tsai, H.-Y.; Yang, M.-F.; Chang, H.-C.; Liu, S.-L.; Kuo, L.-H.; Wang, W.-R.; Yang, P.-A.; Huang, S.-J.; et al. Effect of Charged Amino Acid Side Chain Length on Lateral Cross-Strand Interactions between Carboxylate-Containing Residues and Lysine Analogues in a  $\beta$ -Hairpin. *Biochemistry* **2013**, *52*, 9212–9222. [[CrossRef](#)]
26. Kuo, H.-T.; Liu, S.-L.; Chiu, W.-C.; Fang, C.-J.; Chang, H.-C.; Wang, W.-R.; Yang, P.-A.; Li, J.-H.; Huang, S.-J.; Huang, S.-L.; et al. Effect of charged amino acid side chain length on lateral cross-strand interactions between carboxylate- and guanidinium-containing residues in a  $\beta$ -hairpin. *Amino Acids* **2015**, *47*, 885–898. [[CrossRef](#)] [[PubMed](#)]
27. Huang, C.-H.; Wong, T.W.; Yu, C.-H.; Chang, J.-Y.; Huang, S.-J.; Huang, S.-L.; Cheng, R.P. Swapping the Positions in a Cross-Strand Lateral Ion-Pairing Interaction between Ammonium- and Carboxylate-Containing Residues in a  $\beta$ -Hairpin. *Molecules* **2021**, *26*, 1346. [[CrossRef](#)] [[PubMed](#)]
28. Chothia, C. Conformation of twisted  $\beta$ -pleated sheets in proteins. *J. Mol. Biol.* **1973**, *75*, 295–302. [[CrossRef](#)]

29. Tatko, C.D.; Waters, M.L. The geometry and efficacy of cation- $\pi$  interactions in a diagonal position of a designed  $\beta$ -hairpin. *Protein Sci.* **2003**, *12*, 2443–2452. [[CrossRef](#)]
30. Hughes, R.M.; Waters, M.L. Influence of N-methylation on a cation- $\pi$  interaction produces a remarkably stable  $\beta$ -hairpin peptide. *J. Am. Chem. Soc.* **2005**, *127*, 6518–6519. [[CrossRef](#)]
31. Hughes, R.M.; Waters, M.L. Arginine methylation in a  $\beta$ -hairpin peptide: Implications for Arg- $\pi$  interactions,  $\Delta C_p^0$ , and the cold denatured state. *J. Am. Chem. Soc.* **2006**, *128*, 12735–12742. [[CrossRef](#)]
32. Hughes, R.M.; Benshoff, M.L.; Waters, M.L. Effects of chain length and N-methylation on a cation- $\pi$  interaction in a  $\beta$ -hairpin peptide. *Chem. Eur. J.* **2007**, *13*, 5753–5764. [[CrossRef](#)]
33. Kiehna, S.E.; Laughrey, Z.R.; Waters, M.L. Evaluation of a carbohydrate- $\pi$  interaction in a peptide model system. *Chem. Commun.* **2007**, 4026–4028. [[CrossRef](#)]
34. Laughrey, Z.R.; Kiehna, S.E.; Riemen, A.J.; Waters, M.L. Carbohydrate- $\pi$  interactions: What are they worth? *J. Am. Chem. Soc.* **2008**, *130*, 14625–14633. [[CrossRef](#)]
35. Hughes, R.M.; Waters, M.L. Effects of lysine acetylation in a  $\beta$ -hairpin peptide: Comparison of an amide- $\pi$  and a cation- $\pi$  interaction. *J. Am. Chem. Soc.* **2006**, *128*, 13586–13591. [[CrossRef](#)]
36. Stanger, H.E.; Gellman, S.H. Rules for Antiparallel  $\beta$ -Sheet Design: D-Pro-Gly Is Superior to L-Asn-Gly for  $\beta$ -Hairpin Nucleation1. *J. Am. Chem. Soc.* **1998**, *120*, 4236–4237. [[CrossRef](#)]
37. Syud, F.A.; Espinosa, J.F.; Gellman, S.H. NMR-Based Quantification of  $\beta$ -Sheet Populations in Aqueous Solution through Use of Reference Peptides for the Folded and Unfolded States. *J. Am. Chem. Soc.* **1999**, *121*, 11577–11578. [[CrossRef](#)]
38. Chang, J.-Y.; Li, N.-Z.; Wang, W.-M.; Liu, C.-T.; Yu, C.-H.; Chen, Y.-C.; Lu, D.; Lin, P.-H.; Huang, C.-H.; Kono, O.; et al. Longer charged amino acids favor  $\beta$ -strand formation in hairpin peptides. *J. Pept. Sci.* **2021**, *27*, e3333. [[CrossRef](#)]
39. Atherton, E.; Fox, H.; Harkiss, D.; Logan, C.J.; Sheppard, R.C.; Williams, B.J. A mild procedure for solid phase peptide synthesis: Use of fluorenylmethoxycarbonylamino-acids. *J. Chem. Soc. Chem. Commun.* **1978**, 537–539. [[CrossRef](#)]
40. Fields, G.B.; Noble, R.L. Solid phase peptide synthesis utilizing 9-fluorenylmethoxycarbonyl amino acids. *Int. J. Pept. Protein Res.* **1990**, *35*, 161–214. [[CrossRef](#)]
41. Volkmer-Engert, R.; Landgraf, C.; Schneider-Mergener, J. Charcoal surface-assisted catalysis of intramolecular disulfide bond formation in peptides. *J. Pept. Res.* **1998**, *51*, 365–369. [[CrossRef](#)] [[PubMed](#)]
42. Wüthrich, K. *NMR of Proteins and Nucleic Acids*; John Wiley & Sons: New York, NY, USA, 1986.
43. Ramirez-Alvarado, M.; Blanco, F.J.; Serrano, L. De novo design and structural analysis of a model  $\beta$ -hairpin peptide system. *Nat. Struct. Biol.* **1996**, *3*, 604–612. [[CrossRef](#)] [[PubMed](#)]
44. Russell, S.J.; Blandl, T.; Skelton, N.J.; Cochran, A.G. Stability of Cyclic  $\beta$ -Hairpins: Asymmetric Contributions from Side Chains of a Hydrogen-Bonded Cross-Strand Residue Pair. *J. Am. Chem. Soc.* **2003**, *125*, 388–395. [[CrossRef](#)] [[PubMed](#)]
45. Yao, J.; Dyson, H.; Wright, P.E. Chemical shift dispersion and secondary structure prediction in unfolded and partly folded proteins. *FEBS Lett.* **1997**, *419*, 285–289. [[CrossRef](#)]
46. Dalgarno, D.C.; Levine, B.A.; Williams, R.J.P. Structural information from NMR secondary chemical shifts of peptide  $\alpha$  C-H protons in proteins. *Biosci. Rep.* **1983**, *3*, 443–452. [[CrossRef](#)]
47. Wishart, D.S.; Sykes, B.D.; Richards, F.M. Relationship between nuclear magnetic resonance chemical shift and protein secondary structure. *J. Mol. Biol.* **1991**, *222*, 311–333. [[CrossRef](#)]
48. Kim, Y.; Prestegard, J.H. Measurement of vicinal couplings from cross peaks in COSY spectra. *J. Magn. Reson.* **1989**, *84*, 9–13. [[CrossRef](#)]
49. Pardi, A.; Billeter, M.; Wüthrich, K. Calibration of the angular dependence of the amide proton-C $\alpha$  proton coupling constants,  $^3J_{NH\alpha}$ , in a globular protein. Use of  $^3J_{NH\alpha}$  for identification of helical secondary structure. *J. Mol. Biol.* **1984**, *180*, 741–751. [[CrossRef](#)]
50. Horovitz, A. Double-mutant cycles: A powerful tool for analyzing protein structure and function. *Fold. Des.* **1996**, *1*, R121–R126. [[CrossRef](#)]
51. Stanger, H.E.; Syud, F.A.; Espinosa, J.F.; Giriat, I.; Muir, T.; Gellman, S.H. Length-dependent stability and strand length limits in antiparallel  $\beta$ -sheet secondary structure. *Proc. Natl. Acad. Sci. USA* **2001**, *98*, 12015–12020. [[CrossRef](#)]
52. Bax, A.; Davis, D.G. MLEV-17-based two-dimensional homonuclear magnetization transfer spectroscopy. *J. Magn. Reson.* **1985**, *65*, 355–360. [[CrossRef](#)]
53. Bothner-by, A.A.; Stephens, R.L.; Lee, J.; Warren, C.D.; Jeanloz, R.W. Structure determination of a tetrasaccharide: Transient nuclear Overhauser effects in the rotating frame. *J. Am. Chem. Soc.* **1984**, *106*, 811–813. [[CrossRef](#)]
54. Aue, W.P.; Bartholdi, E.; Ernst, R.R. Two-dimensional spectroscopy. Application to nuclear magnetic resonance. *J. Chem. Phys.* **1976**, *64*, 2229–2246. [[CrossRef](#)]
55. Piotto, M.; Saudek, V.; Sklenar, V. Gradient-tailored excitation for single-quantum NMR spectroscopy of aqueous solutions. *J. Biomol. NMR* **1992**, *2*, 661–665. [[CrossRef](#)]
56. Butterfield, S.M.; Waters, M.L. A Designed  $\beta$ -Hairpin Peptide for Molecular Recognition of ATP in Water. *J. Am. Chem. Soc.* **2003**, *125*, 9580–9581. [[CrossRef](#)]
57. Butterfield, S.M.; Cooper, W.J.; Waters, M.L. Minimalist Protein Design: A  $\beta$ -Hairpin Peptide That Binds ssDNA. *J. Am. Chem. Soc.* **2005**, *127*, 24–25. [[CrossRef](#)]

58. Stewart, A.L.; Waters, M.L. Structural Effects on ss- and dsDNA Recognition by a  $\beta$ -Hairpin Peptide. *ChemBioChem* **2009**, *10*, 539–544. [[CrossRef](#)]
59. Hamy, F.; Felder, E.R.; Heizmann, G.; Lazdins, J.; Aboul-Ela, F.; Varani, G.; Karn, J.; Klimkait, T. An inhibitor of the Tat/TAR RNA interaction that effectively suppresses HIV-1 replication. *Proc. Natl. Acad. Sci. USA* **1997**, *94*, 3548–3553. [[CrossRef](#)]
60. Runyon, S.T.; Puglisi, J.D. Design of a Cyclic Peptide that Targets a Viral RNA. *J. Am. Chem. Soc.* **2003**, *125*, 15704–15705. [[CrossRef](#)]
61. Athanassiou, Z.; Dias, R.L.A.; Moehle, K.; Dobson, N.; Varani, G.; Robinson, J.A. Structural mimicry of retroviral Tat proteins by constrained  $\beta$ -hairpin peptidomimetics: Ligands with high affinity and selectivity for viral TAR RNA regulatory elements. *J. Am. Chem. Soc.* **2004**, *126*, 6906–6913. [[CrossRef](#)]
62. Moehle, K.; Athanassiou, Z.; Patora, K.; Davidson, A.; Varani, G.; Robinson, J.A. Design of  $\beta$ -Hairpin Peptidomimetics That Inhibit Binding of  $\alpha$ -Helical HIV-1 Rev Protein to the Rev Response Element RNA. *Angew. Chem. Int. Ed.* **2007**, *46*, 9101–9104. [[CrossRef](#)]
63. Davidson, A.; Leeper, T.C.; Athanassiou, Z.; Patora-Komisarska, K.; Karn, J.; Robinson, J.A.; Varani, G. Simultaneous recognition of HIV-1 TAR RNA bulge and loop sequences by cyclic peptide mimics of Tat protein. *Proc. Natl. Acad. Sci. USA* **2009**, *106*, 11931–11936. [[CrossRef](#)]
64. Cline, L.L.; Waters, M.L. Design of a  $\beta$ -hairpin peptide-intercalator conjugate for simultaneous recognition of single stranded and double stranded regions of RNA. *Org. Biomol. Chem.* **2009**, *7*, 4622–4630. [[CrossRef](#)]
65. Drakopoulou, E.; Zinn-Justin, S.; Guenneugues, M.; Gilquin, B.; Ménez, A.; Vita, C. Changing the structural context of a functional  $\beta$ -hairpin. *J. Biol. Chem.* **1996**, *271*, 11979–11987. [[CrossRef](#)]
66. González-Navarro, H.; Mora, P.; Pastor, M.; Serrano, L.; Mingarro, I.; Pérez-Payá, E. Identification of peptides that neutralize bacterial endotoxins using  $\beta$ -hairpin conformationally restricted libraries. *Mol. Divers.* **2000**, *5*, 117–126. [[CrossRef](#)]
67. Lai, J.R.; Huck, B.R.; Weisblum, B.; Gellman, S.H. Design of Non-Cysteine-Containing Antimicrobial  $\beta$ -Hairpins: Structure–Activity Relationship Studies with Linear Protegrin-1 Analogues. *Biochemistry* **2002**, *41*, 12835–12842. [[CrossRef](#)]
68. Schneider, J.P.; Pochan, D.J.; Ozbas, B.; Rajagopal, K.; Pakstis, L.; Kretsinger, J. Responsive Hydrogels from the Intramolecular Folding and Self-Assembly of a Designed Peptide. *J. Am. Chem. Soc.* **2002**, *124*, 15030–15037. [[CrossRef](#)]
69. Pochan, D.J.; Schneider, J.P.; Kretsinger, J.; Ozbas, B.; Rajagopal, K.; Haines, L. Thermally Reversible Hydrogels via Intramolecular Folding and Consequent Self-Assembly of a de Novo Designed Peptide. *J. Am. Chem. Soc.* **2003**, *125*, 11802–11803. [[CrossRef](#)] [[PubMed](#)]
70. Salick, D.A.; Kretsinger, J.K.; Pochan, D.J.; Schneider, J.P. Inherent Antibacterial Activity of a Peptide-Based  $\beta$ -Hairpin Hydrogel. *J. Am. Chem. Soc.* **2007**, *129*, 14793–14799. [[CrossRef](#)]
71. Haines-Butterick, L.; Rajagopal, K.; Branco, M.; Salick, D.; Rughani, R.; Pilarz, M.; Lamm, M.S.; Pochan, D.J.; Schneider, J.P. Controlling hydrogelation kinetics by peptide design for three-dimensional encapsulation and injectable delivery of cells. *Proc. Natl. Acad. Sci. USA* **2007**, *104*, 7791–7796. [[CrossRef](#)]
72. Nagarkar, R.P.; Hule, R.A.; Pochan, D.J.; Schneider, J.P. De Novo Design of Strand-Swapped  $\beta$ -Hairpin Hydrogels. *J. Am. Chem. Soc.* **2008**, *130*, 4466–4474. [[CrossRef](#)] [[PubMed](#)]
73. Medina, S.H.; Li, S.; Howard, O.M.Z.; Dunlap, M.; Trivett, A.; Schneider, J.P.; Oppenheim, J.J. Enhanced immunostimulatory effects of DNA-encapsulated peptide hydrogels. *Biomaterials* **2015**, *53*, 545–553. [[CrossRef](#)] [[PubMed](#)]
74. Nagy-Smith, K.; Moore, E.; Schneider, J.; Tycko, R. Molecular structure of monomeric peptide fibrils within a kinetically trapped hydrogel network. *Proc. Natl. Acad. Sci. USA* **2015**, *112*, 9816–9821. [[CrossRef](#)] [[PubMed](#)]
75. Yamada, Y.; Schneider, J.P. Fragmentation of Injectable Bioadhesive Hydrogels Affords Chemotherapeutic Macromolecules. *Biomacromolecules* **2016**, *17*, 2634–2641. [[CrossRef](#)]
76. Medina, S.H.; Schneider, J.P. Cancer cell surface induced peptide folding allows intracellular translocation of drug. *J. Control. Release* **2015**, *209*, 317–326. [[CrossRef](#)]
77. Medina, S.H.; Miller, S.E.; Keim, A.I.; Gorka, A.P.; Schnermann, M.J.; Schneider, J.P. An Intrinsically Disordered Peptide Facilitates Non-Endosomal Cell Entry. *Angew. Chem. Int. Ed.* **2016**, *55*, 3369–3372. [[CrossRef](#)]
78. Cheng, Y.-S.; Chen, Z.-T.; Liao, T.-Y.; Lin, C.; Shen, H.C.-H.; Wang, Y.-H.; Chang, C.-W.; Liu, R.-S.; Chen, R.P.-Y.; Tu, P.-H. An intranasally delivered peptide drug ameliorates cognitive decline in Alzheimer transgenic mice. *EMBO Mol. Med.* **2017**, *9*, 703–715. [[CrossRef](#)]
79. Watkins, A.M.; Arora, P.S. Anatomy of  $\beta$ -strands at protein-protein interfaces. *ACS Chem. Biol.* **2014**, *9*, 1747–1754. [[CrossRef](#)]
80. Blosser, S.L.; Sawyer, N.; Maksimovic, I.; Ghosh, B.; Arora, P.S. Covalent and noncovalent targeting of the Tcf4/ $\beta$ -catenin strand interface with  $\beta$ -hairpin mimics. *ACS Chem. Biol.* **2021**, *16*, 1518–1525. [[CrossRef](#)]